JACS
JOURNAL OF THE AMERICAN CHEMICAL SOCIETY
Article
pubs.acs.org/JACS

Adsorbate-Induced Structural Changes in 1−3 nm Platinum Nanoparticles

Yu Lei,[∥,¶] Haiyan Zhao,[‡,¶] Rosa Diaz Rivas,[⊥] Sungsik Lee,[‡] Bin Liu,[#] Junling Lu,[†] Eric Stach,[⊥] Randall E. Winans,[‡] Karena W. Chapman,[‡] Jeffrey P. Greeley,[⊗] Jeffrey T. Miller,[§] Peter J. Chupas,[‡] and Jeffrey W. Elam*[,†]

[†]Energy Systems Division, [‡]X-ray Science Division, [§]Chemical Sciences and Engineering Division, Argonne National Laboratory, Lemont, Illinois 60439, United States

[∥]Department of Chemical and Materials Engineering, University of Alabama in Huntsville, Huntsville, Alabama 35899, United States

[⊥]Center for Functional Nanomaterials, Brookhaven National Laboratory, Upton, New York 11973, United States

[#]Department of Chemical Engineering, Kansas State University, Manhattan, Kansas 66506, United States

[⊗]Department of Chemical Engineering, Purdue University, West Lafayette, Indiana 47907, United States

Supporting Information

ABSTRACT: We investigated changes in the Pt−Pt bond distance, particle size, crystallinity, and coordination of Pt nanoparticles as a function of particle size (1−3 nm) and adsorbate (H_2, CO) using synchrotron radiation pair distribution function (PDF) and X-ray absorption spectroscopy (XAS) measurements. The ∼1 nm Pt nanoparticles showed a Pt−Pt bond distance contraction of ∼1.4%. The adsorption of H_2 and CO at room temperature relaxed the Pt−Pt bond distance contraction to a value close to that of bulk fcc Pt. The adsorption of H_2 improved the crystallinity of the small Pt nanoparticles. However, CO adsorption generated a more disordered fcc structure for the 1−3 nm Pt nanoparticles compared to the H_2 adsorption Pt nanoparticles. *In situ* XANES measurements revealed that this disorder results from the electron back-donation of the Pt nanoparticles to CO, leading to a higher degree of rehybridization of the metal orbitals in the Pt-adsorbate system.

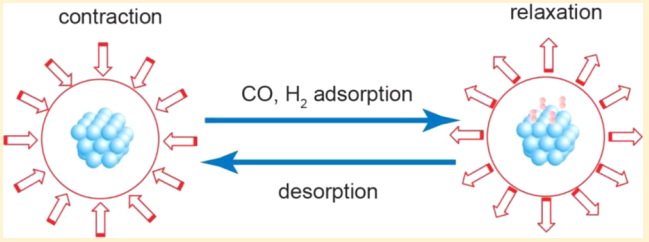

INTRODUCTION

Metal nanoparticles can exhibit dramatically different chemical and physical properties compared to their bulk counterparts.[1−4] Owing to their highly under-coordinated surfaces, small metal nanoparticles in the sub-10 nm range play an important role in industrial heterogeneous catalysis.[5−7] The structure of the supported metal nanoparticles can change dynamically under reaction condition such as when molecules adsorb on the surface. A fundamental understanding of the structure of supported sub-10 nm metal nanoparticles, under reaction conditions, is an important step toward achieving precise structure−reactivity relationship in heterogeneous catalysis and will ultimately lead to better catalysts.

Prominent features of sub-10 nm diameter metal nanoparticles include a contracted lattice parameter and higher structural disorder with decreasing particle size. Lennard-Jones first predicted that a small contraction (5−6%) may occur in the surface layer of a crystal due to surface-tension in 1928.[8] In the 1930s, scientists found discrepancies between the lattice constants of zinc oxide and alkali halides obtained by electron diffraction and X-ray diffraction, respectively. Bunn suggested that these differences were due to a change in the lattice constants of zinc oxide at the surface, since electron diffraction was more surface sensitive than X-ray diffraction.[9] Finch and Fordham found that some small alkali halide crystals had larger lattice constants than their bulk counterparts.[10] Since then, debate over the origin of lattice contraction and expansion has persisted. In the 1950s, the debate was eventually settled when lattice contraction in small particles was determined in alkali halides and metals.[11,12] This contraction increased with decreasing particle size for particles below 10 nm in diameter.[11] It was also realized that the structure and shape of very small particles may not be the same as their bulk counterparts,[12] which could lead to incorrect interpretations of diffraction results. Consequently, an advanced technique is desired to provide bond-length information independent of materials crystal structure.

With the development of X-ray absorption spectroscopy (XAS) in the 1970s, it was discovered that the nearest-neighbor bond distance decreased with decreasing particle size for Cu and Ni using extended X-ray absorption fine structure (EXAFS).[13] A similar trend was also found for supported precious metal nanoparticles.[14,15] A 5% contraction was observed for supported, 1 nm Au and Pt nanoparticles independent of the supports.

Received: December 13, 2013
Published: June 12, 2014

   dx.doi.org/10.1021/ja4126998 | *J. Am. Chem. Soc.* 2014, 136, 9320−9326

However, Norskov and co-workers cast doubt on the EXAFS measurement at room temperature after calculating the pair distribution function (PDF) of Cu clusters with 100−1000 atoms using molecular-dynamics simulations. They suggested that the observed lattice contraction was due to anharmonic vibrations of the surface atoms at room temperature.[16] More recently, van Bokhoven and co-workers performed *in situ* EXAFS on supported Pt nanoparticles between 77 and 673 K. Accurate fittings were obtained for their EXAFS spectra at elevated temperature by including the third and fourth cumulants in the amplitude and phase of the EXAFS functions, where changes in the Debye−Waller factor due to asymmetry and sharpening or broadening of the PDF were considered.[17] However, including the third and fourth cumulants could also easily lead to overfitting, that is, applying too many variables.

In recent years, the synchrotron X-ray PDF has emerged as an important tool to investigate supported catalysts at the atomic scale.[18,19] Unlike EXAFS data analysis which is limited to the first few neighbor shells, PDF provides quantitative structural information on both the short- and long-range order of small nanoparticles.[20,21] The PDF, $G(r)$, can be obtained by Fourier transforming the normalized scattering function, $S(Q)$, so that no intensive data fitting is required.

In this work, we combined PDF and XAS measurements to reveal the lattice contraction and expansion of supported small platinum nanoparticles as a function of the particle size and the adsorbate. Our previous X-ray absorption near edge structure (XANES) study on Pt nanoparticles supported on different surfaces showed that the support effects with respect to lattice constants were minimal at constant Pt nanoparticle size. [15] Thus, in this work, we focused on 1−3 nm Pt nanoparticles supported on spherical alumina. This spherical alumina support facilitates transmission electron microscopy (TEM) measurements.

EXPERIMENTAL DETAILS

Preparation of 1−3 nm Pt Nanoparticles. Supported platinum nanoparticles were prepared by atomic layer deposition (ALD). All the Pt samples were prepared in a continuous-flow stainless steel reactor operated under a base pressure of ∼ 1 Torr.[22] Spherical alumina nanopowder (Al_2O_3, Alfa-Aesar NanoDur) with a typical particle diameter of 40−50 nm and surface area of 32−40 m^2/g were used as the support material. Five hundred milligrams of Al_2O_3 was evenly spread into a flat stainless steel tray and loaded into the ALD reactor. Before performing the Pt ALD, the Al_2O_3 was first cleaned *in situ* using 400 sccm 10% ozone at 523 K. Pt ALD was performed using trimethyl(methylcyclopentadienyl)platinum (IV) (Pt(MeCp)Me_3, Sigma-Aldrich) and oxygen. Three samples were prepared using 1, 3, and 5 Pt ALD cycles over Al_2O_3, written as 1c Pt/Al_2O_3, 3c Pt/Al_2O_3, and 5c Pt/Al_2O_3, respectively.

Characterization. An aberration-corrected transmission electron microscope, FEI Titan 80−300 kV, was used for imaging. High resolution TEM images were acquired at 300 kV with a base pressure of 5×10^{-7} Torr at room temperature using a Gatan UltraScan CCD camera. Pt metal loadings were determined by X-ray fluorescence spectroscopy (XRF, Oxford ED2000) and inductively coupled plasma (ICP, Varian Vista-MPX instrument) measurements.

Pair Distribution Function. Scattering data of PDF were collected at beamline 11-ID-B at the Advanced Photon Source (APS) at Argonne National Laboratory (ANL). High energy X-rays (58 keV, λ = 0.2127Å) were used in combination with a large amorphous silicon-based area detector. The Pt catalyst was loaded into a Kapton capillary as a flow cell which allowed the flow of reactant gases during the *in situ* PDF measurements.[23] Temperature was precisely controlled by a cryosystem (Oxford, Cryostream 700 Plus). The as-prepared Pt catalysts (Pt-in-air) were first reduced in 3.5% H_2/He at 500 K for 30 min. Then ultrahigh purity (UHP) He was used to purge the catalyst for 30 min at 500 K to generate the ligand-free Pt surface (Pt-in-He). The Pt sample was then cooled in UHP He to 300 K and subsequently exposed to 3.5% H_2/He for hydrogen adsorption (Pt-in-H_2). The Pt sample then was again flashed to 500 at 6 K/min and cooled in UHP He. Finally, the sample was exposed to 5% CO/He for CO adsorption (Pt-in-CO). PDF measurements were collected continuousy during the entire sample treatment.

The 2-D scattering images were integrated to obtain 1-D scattering intensity data using software Fit2D.[24] The structure function $S(Q)$ was obtained within software PDFgetX2.[25] Direct Fourier transform of the reduced structure function $F(Q) = Q[S(Q) - 1]$ led to the reduced pair distribution function, $G(r)$, with Q_{max} = 23 $Å^{-1}$. Contributions from the Al_2O_3 support were measured from room temperature to 500 K and subtracted to yield differential PDF (*d*-PDF). The *d*-PDF data will show contributions only from Pt-atom correlations.

X-ray Absorption Spectroscopy (XAS). X-ray absorption spectroscopy measurements at the Pt L_3 edge (∼11.56 keV), including extended X-ray absorption fine structure spectroscopy (EXAFS) and X-ray absorption near edge structure spectroscopy (XANES), were performed at the bending-magnet beamline (10-BM) of the Materials Research Collaborative Access Team (MR-CAT) at the APS at ANL. XAS data was collected in the transmission mode. Pt nanoparticle samples were treated identically as that used in the *in situ* PDF experiments described above.

EXAFS data fittings were performed using WinXAS (version 3.1). Reference phase and amplitude files for Pt−Pt were obtained from the Pt foil EXAFS spectrum. A single shell model fit of the forward and inverse k^2-weighted EXAFS data was obtained between k = 2.9−11.0 $Å^{-1}$ and r = 1.3−3.0 Å, respectively. Data quality was checked by performing k^1- and k^3-weighted EXAFS fittings with the same parameters.

Small Angle X-ray Scattering (SAXS). SAXS experiments were performed at the APS 12-ID-B station. The Pt catalyst samples were loaded into 1.5-mm diameter quartz capillary tubes for the SAXS measurements. The 2D SAXS data were collected on the Pilatus 2 M area detector (DECTRIS Ltd.), a q range of 0.006 − 0.7 $Å^{-1}$ with an incident energy of 12 keV. The scattering vector, Q, was calibrated using a silver behenate. Quantitative data analyses were performed using spherical form factors with a maximum entropy algorithm using the Irena package. [26]

Classical Molecular Dynamics (MD) Simulations. The MD simulations were performed using the DL_POLY 2.20 package. [27] The Al−Al, O−O, Al−O interactions within the alumina slab were described using the Buckingham pair-potential, using the parameters provided by Matsui et al. [28] The Pt−Pt interactions were treated with the Sutton-Chen potential.[29,30] The Pt−Al and Pt−O interactions between metal and the substrate were treated with the Lennard-Jones potential (see Table S2 in Supporting Information).[31,32]

The alumina support was modeled using a stoichiometric α-Al_2O_3 slab with the (001) surface. The slab consists of 6 layers, with 1080 atoms. The entire system is maintained charge neutral. The dimensions of the alumina slab are 24.85 Å × 28.69 Å × 50.00 Å, and is periodically bounded. The consecutive surfaces are separated by a vacuum spacing equivalent to a thickness of 12 layers.

To calculate the PDFs of both supported and unsupported Pt nanoparticles, the simulations were carried out in microcanonical ensembles. The cutoff radius for both short-range forces and the van der Waals forces was selected to be 12.3. The Ewald sum for electrostatic interactions was used and the precision is set to be 1×10^{-6}. The velocity-Verlet integration algorithm was used for time propagation with a time step of 1 fs. All the simulations were initially equilibrated at 500 K for 100 ps. The PDFs were averaged based on the last 50 000 configurations. All the atoms are allowed to relax during the simulation.

RESULTS AND DISCUSSION

Studies of small changes in bond distance require highly dispersed and ligand-free supported Pt nanoparticles with

dx.doi.org/10.1021/ja4126998 | J. Am. Chem. Soc. 2014, 136, 9320−9326

narrow size distribution. Atomic layer deposition has proved effective in preparing well-dispersed, precious metal nanoparticles on high surface area supports using sequential, self-limiting surface reactions.[33,34] We used alternating exposures to Pt(MeCp)Me_3 and oxygen at 523 K to prepare supported ALD Pt nanoparticles. One, three, and five Pt ALD cycles were performed on spherical alumina (Al_2O_3) in a continuous-flow, stainless steel reactor operated under a base pressure of ~1 Torr UHP nitrogen carrier gas. [22] The Pt for the 1c, 3c and 5c samples were 1.4, 8.7, and 16 wt %, respectively, as determined by X-ray fluorescence spectroscopy (XRF). These loadings are lower than those obtained previously at 573 K (2.5 wt % for 1c Pt and 10.4 wt % for 3c Pt).[35,36] This change is expected given that the ALD Pt growth per cycle decreases with decreasing temperature. [37] We selected the 523K deposition temperature because it produced smaller particles with a narrower size distribution. We determined the Pt nanoparticle size using TEM, SAXS, and PDF, (Table 1) and found consistent results among the three techniques.

Table 1. Platinum Metal Loading and Particle Size Determined by Various Methods.

	Pt loading wt %[a]	d_{Pt} (TEM) (nm)[b]	d_{Pt} (SAXS) (nm)[c]	d_{Pt} (PDF) (nm)[d]
1c Pt	1.4	1 ± 0.3	1.2	1.2
3c Pt	8.7	2 ± 0.5	2.2	2.4
5c Pt	16.0	3 ± 0.6	3.2	3.4

[a]Obtained by XRF and ICP. [b]Obtained by TEM (Figure 1). [c]Obtained by small-angle X-ray scattering (Figure 2). [d]Obtained by pair distribution function (Figure S2).

The Pt nanoparticles were well-dispersed on the Al_2O_3 surface (Figure 1) with particle size distributions of 1 ± 0.3, 2 ± 0.5, and 3 ± 0.6 nm for the 1c, 3c, and 5c Pt samples, respectively. These sizes are smaller than the Pt prepared at 573 K on the same support. [35] High resolution TEM (HR-TEM) imaging was used to determine the shape and crystallinity of the supported Pt nanoparticles. Figure 1b,d shows HR-TEM images of the 1c and 3c Pt nanoparticle samples on Al_2O_3. The 3c sample formed truncated octahedra with widths around 2 ± 0.5 nm and distance between the lattice fringes of 0.2 nm corresponds to the interplanar distance of Pt(100).

The Pt particle size was also evaluated using SAXS measurements. Figure 2a shows the 1-D scattering curves obtained from 2-D SAXS measurements. The broad features on the curves shifted to lower q values with increasing Pt ALD cycles, consistent with an increase in the Pt particle size. The particle sizes extracted from the SAXS measurements for the as-prepared Pt nanoparticles are 1.2 nm, 2.2 nm, and 3.2 nm for the 1c, 3c, and 5c Pt samples, respectively.

Differential PDF (*d*-PDF) is an analytical technique in which the contribution from the support is subtracted from the total PDF, leaving only the atom-atom correlations from the supported particles.[20,38,39] PDF measurements were performed on the Al_2O_3 support from 300 to 500 K at 6 K/min to serve as a reference for the subsequent *d*-PDFs data analysis. Figure S1 demonstrates that the change in Al_2O_3 structure over this temperature range is negligible. After the Al_2O_3 PDF data is substracted, the resulting *d*-PDF plots in Figure 3 reveal a series of sharp peaks, each reflecting a particular atom-atom correlation (e.g., Pt−Pt and Pt−O). The peaks at around 2.78, 3.95, and 4.75 Å are characteristic of the Pt fcc structure.

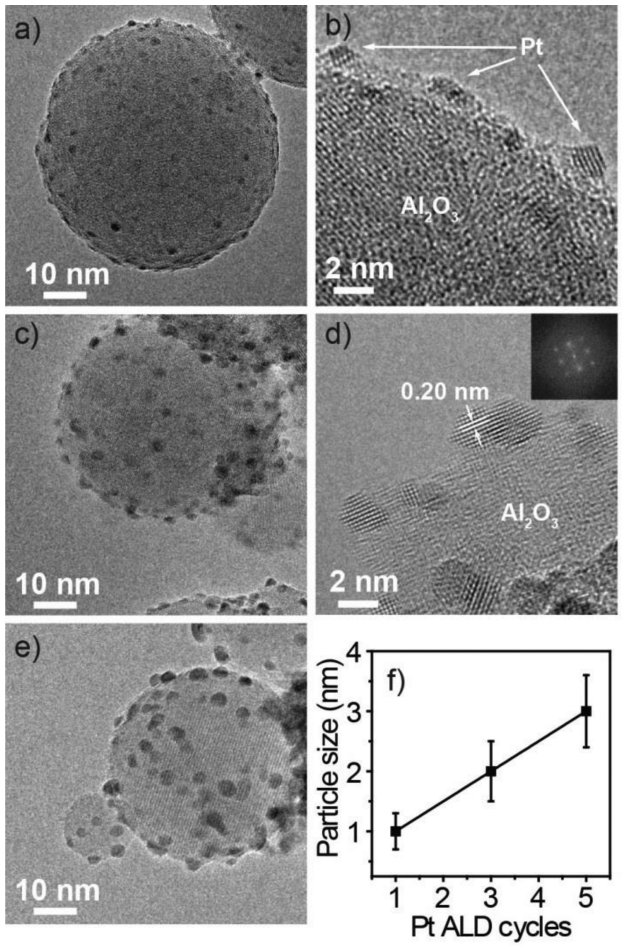

Figure 1. (a) TEM and (b) HR-TEM images of 1c Pt/Al_2O_3; (c) TEM and (d) HR-TEM images of 3c Pt/Al_2O_3 with FFT shown in the insert; (e) TEM image of 5c Pt/Al_2O_3; (f) size distribution of Pt nanoparticles.

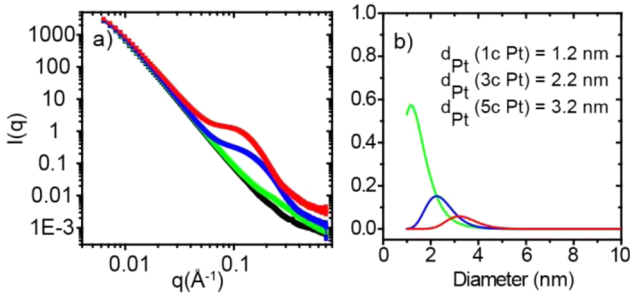

Figure 2. (a) One-dimensional SAXS curves of Pt/Al_2O_3 and bare Al_2O_3 resulting from average the 2D diffraction image; (b) size distribution of the as-prepared Pt nanoparticles obtained from SAXS modeling. Black, Al_2O_3; green, 1c Pt/Al_2O_3; blue, 3c Pt/Al_2O_3; red, 5c Pt/Al_2O_3.

These peaks decay to zero faster for smaller Pt particles, reflecting the absence of large-scale correlations in these particles. In particular, there are no features in the *d*-PDF data beyond $r \approx 1.0$ nm for the 1c Pt sample, suggesting that there are no particles larger than ~1 nm. As for the 3c and 5c Pt samples, the nanoparticle sizes are estimated as ~2 and ~3 nm, respectively.

As PDF uses high energy X-rays (58 keV in this work), the effect of beam damage to the samples, i.e., possible sintering of

dx.doi.org/10.1021/ja4126998 | J. Am. Chem. Soc. 2014, 136, 9320−9326

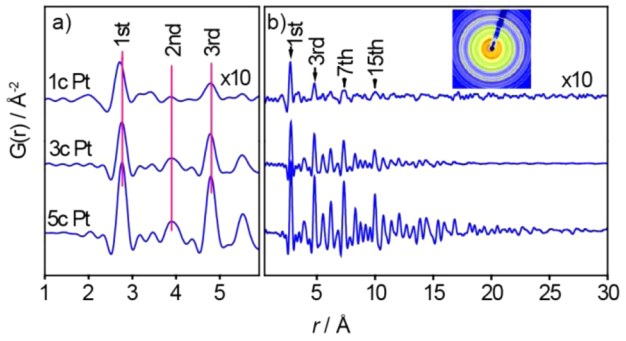

Figure 3. Differential PDFs for as-prepared 1c Pt/Al_2O_3, 3c Pt/Al_2O_3, and 5c Pt/Al_2O_3 measured under ambient conditions, resulting from integration of the 2D diffraction images (representative image shown in the inset).

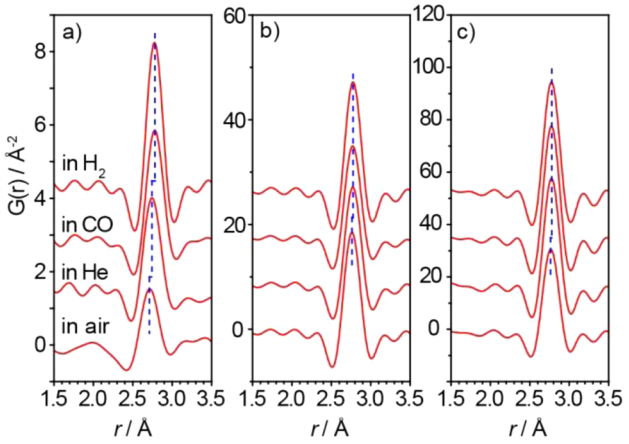

Figure 4. Differential PDFs for (a) 1c Pt/Al_2O_3, (b) 3c Pt/Al_2O_3, and (c) 5c Pt/Al_2O_3 under different conditions.

Pt nanoparticles caused by high energy X-rays, was examined prior to the *in situ* adsorption experiments. The samples were constantly exposed to 58 keV X-rays for two hours at room temperature and PDFs were taken simultaneously. No obvious change of the size of Pt nanoparticles was observed.

For all of the as-prepared samples, there is a small, broad peak at about 2.00 Å corresponding to scattering from the Pt-O pair. This suggests that the as-prepared Pt nanoparticles are partially oxidized on the surface. Because oxygen is a low Z element, the scattering from Pt-O is relatively weak compared to Pt−Pt. [40] Precise particle size was obtained from quantitative fitting of the *d*-PDF data from the Pt-in-He using software PDFgui [25] by applying a fcc Pt structure with spherical shape. As shown in Figure S2, the particle sizes obtained were 1.2, 2.4, and 3.4 nm for 1c, 3c, and 5c Pt, respectively. These values from the *d*-PDF data are consistent with those obtained from TEM and SAXS.

As mentioned above, it is important to use ligand free Pt nanoparticles to obtain unambiguous results on the effect of adsorbates. However, the as-prepared 1−3 nm Pt nanoparticles were likely partially or fully oxidized during the sample transfer and the gap between sample preparation and analysis. In addition, it was reported that for precious metal nanoparticles in this size regime, degree of oxidation increased with decreasing Pt particle size and increasing percentage of surface atoms. [41] It was indeed the case from XAS measurements on the as-prepared Pt nanoparticle samples (Figure S3). The as-prepared Pt samples all showed clear Pt−O pair scattering in the R-space of EXAFS spectra. In particular, for 1c Pt/Al_2O_3 which had the smallest Pt particle size among all samples, Pt−O is the dominant feature in its EXAFS spectrum. Therefore, in this work, the Pt nanoparticles samples were fully reduced by H_2 at 500 K and protected in He in the *in situ* sample cell at the beamline prior to the gas molecule adsorption experiments for both PDF and XAS measurements.

Figure 4 shows the *d*-PDF data measured for the 1c, 3c, and 5c samples in various states: as-prepared (Pt-in-air), H_2-reduced and protected in He (Pt-in-He), in H_2, and in CO. The literature value for the Pt−Pt bond distance in bulk Pt is 2.78 Å. [42] As shown in Figure 4a, the as-prepared 1c Pt sample has a first shell Pt−Pt bond distance of 2.72 Å. The as-prepared Pt was then fully reduced in 3.5% H_2 at 500 K for 30 min. The cell was then evacuated, backfilled with UHP helium at 500 K to completely remove hydrogen from the supported Pt nanoparticles (Pt-in-He), and cooled to room temperature. The Pt−Pt bond distance of the ∼1 nm Pt-in-He nanoparticles measured at room temperature was 2.74 Å, a ∼1.4% contraction with respect to the bulk value. Next, the Pt-in-He nanoparticles were exposed to 3.5% H_2/He and 5% CO/He, respectively, to study the effects of these adsorbates on the Pt−Pt bond distance. Upon adsorption of the H_2 and CO, the Pt−Pt bond distance relaxed to 2.77 and 2.78 Å, respectively, close to the bulk Pt value. After the adsorption experiments, the supported Pt nanoparticles were reoxidized by annealing in 5% O_2/He at 500 K. The bond distance again contracted to 2.70 Å, indicating no sintering of the Pt nanoparticles during the various treatments. Moreover, the even shorter distance compared to the as-prepared value suggests an even smaller Pt metal core following the O_2 treatment than for the as-prepared, partially oxidized Pt particles. As shown in Figure 4b,c, the PDF measurements for the contraction and relaxation effects on the 2−3 nm Pt nanoparticles are relatively small compared to the 1 nm sample. For the as-prepared samples, the Pt−Pt bond distance contracted only slightly to 2.77 Å. The 2−3 nm Pt-in-He nanoparticles with and without adsorbates exhibited the bulk Pt−Pt bond distance of 2.78 Å. Sintering was not observed for any of the Pt samples during the adsorption experiments in the *d*-PDFs shown in Figure S4.

The contraction and relaxation of the Pt−Pt bond distance can be clearly observed from the outer shell of Pt. The first, third, seventh, and 15th Pt−Pt shells are major peaks in the Pt PDF data, and these distances are summarized in Table S1 and Figure 5. The 15th shell, corresponding to a Pt−Pt distance of ∼10 Å, is similar to the average size of the 1c Pt nanoparticles. Consequently, the changes in this Pt−Pt pair can be considered the contraction and expansion of the whole Pt nanoparticle. For the 1c Pt-in-He, this shell shows a slight contraction of ∼0.3% with respect to bulk. Upon H_2 adsorption, the particles show a slight expansion of ∼0.1% with respect to the bulk. When CO was adsorbed, the whole Pt nanoparticles exhibited ∼0.3% expansion with respect to the bulk.

The shape and intensity of the peaks in the PDFs directly correlate to the anisotropy of the 1−3 nm Pt nanoparticles. A change induced by adsorbates is the crystallinity in the Pt nanoparticles, which can be described by the full width at half-maximum (fwhm) of the Pt−Pt bond distance at ∼ 2.78 Å.[43] In Figure 5b, the fwhm for the Pt-in-He is in the order of 1c Pt > 3c Pt > 5c Pt. This suggests smaller Pt nanoparticles have a higher degree of disordered nature. The fwhm of Pt-in-H_2 is smaller than the Pt-in-He. This indicates that the adsorption of

dx.doi.org/10.1021/ja4126998 | J. Am. Chem. Soc. 2014, 136, 9320−9326

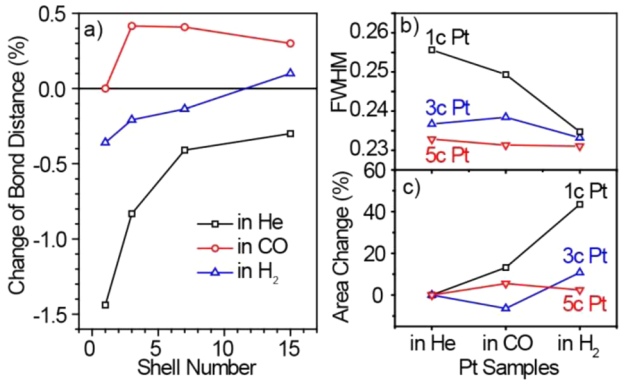

Figure 5. (a) Pt−Pt bond distance expansion and contraction obtained from *d*-PDFs for 1c Pt/Al_2O_3 for reduced Pt, with adsorbed CO and with adsorbed H_2, respectively, with respect to Pt bulk value. (b) Full width at half-maximum (fwhm) and (c) area of the first Pt−Pt peak at ~2.78 Å expansion and contraction obtained from *d*-PDFs for Pt-in-He, with adsorbed CO and with adsorbed H_2, respectively.

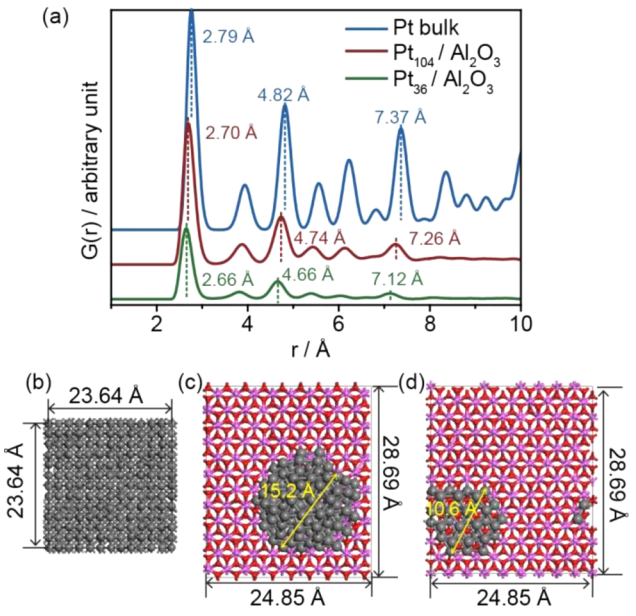

Figure 6. (a) PDFs, $G(r)$, for Pt bulk (blue), Pt_{104} on substrate (red), and Pt_{36} on substrate (green), respectively; (b) bulk Pt structure at optimal lattice constants; (c) Pt_{104} on alumina substrate; (d) Pt_{36} on alumina substrate. Dashed lines indicate the peak locations for the 1st, 3rd, and 7th shells.

H_2 enhances the crystallinity of smaller Pt nanoparticles. Yang and co-workers also observed similar phenomena using a combination of HR-TEM, EXAFS and density functional theory (DFT) studies.[44] Surprisingly, CO adsorption would not only lead to larger Pt−Pt bond relaxation but also larger fwhm than H_2 adsorption, implying greater disorder of Pt nanoparticles.

It was suggested that the contraction of small Pt nanoparticles was due to under-coordination of the surface Pt atoms.[45,46] Adsorbates, such as CO and H_2, would increase the coordination of Pt atoms thereby relaxing the contraction. This hypothesis is indeed supported by our PDF results. The Pt−Pt coordination can be quantified by using the area of the peak at 2.78 Å shown in Figure 5c. The effect is most significant for the ~1 nm particles since virtually all of the Pt atoms are at the surface. Upon adsorption of CO and H_2, the 2.78 Å peak area increased by ~13% and ~44%, respectively. The greater increase in the area of the first-shell of Pt-in-H_2 than Pt-in-CO without increasing particle size (no change in r_{max}) indicates larger increase in coordination numbers of Pt−Pt in H_2 than in CO. In contrast, the changes in peak area for the 3c and 5c samples were much smaller in the presence of CO and H_2 since most of the Pt atoms in these larger particles are already fully coordinated.

Molecular dynamics simulations based on empirical interatomic potentials were used to gain further insights in the structures of supported Pt nanoparticles, and to provide additional evidence for the Pt−Pt bond contractions of supported Pt nanoparticles. The simulated PDFs, $G(r)$, for Pt-bulk and Pt_{104} and Pt_{36} on alumina substrates are shown in Figure 6a, and the corresponding molecular structures of Pt bulk, Pt_{104} ($d \approx 1.5$ nm) and Pt_{36} ($d \approx 1$ nm) are illustrated in Figure 6b−d, respectively. For Pt bulk, the respective Pt−Pt distances for the main peaks at the first, third, and seventh shell are 2.79, 4.82, and 7.37 Å (as labeled in Figure 6). For equilibrated Pt_{104} and Pt_{36}, the Pt atoms organized themselves into islands with each layer arranged based on the fcc ABC-type stacking, resembling that of the Pt bulk. All the peak locations in $G(r)$ corresponding to their respective first, third, and seventh shells move to the left relative to the peaks of Pt bulk, indicating Pt−Pt bond contraction. The Pt−Pt bond distance for each shell follows the order of Pt_{36} < Pt_{104} < Pt bulk. The peak locations of the Pt_{104} cluster show good numerical agreement with the shell distances for 1c Pt/Al_2O_3 in He condition in Table S1.

The structures of free Pt_{104} and Pt_{36} clusters (without support) were also considered using the Sutton-Chen potential (see Figure S5 in Supporting Information). It can be seen that the contraction of the nearest neighbor (first shell) are actually comparable between the particles of the same size, e.g., first shell Pt−Pt distance of 2.65 versus 2.66 Å for Pt_{36}, and first shell Pt−Pt distance of 2.70 versus 2.70 Å for Pt_{104}. What distinguishes the free and supported Pt particles are their geometries: without support the Pt atoms in the cluster are more disordered, as reflected in the PDFs with less pronounced peak features and more severe Pt−Pt bond contractions especially in the outer shells (third and seventh shells). It is also obvious that on the substrate the Pt_{36} cluster shows a *flatter* geometry (with only two atomic layers) compared to Pt_{104} (as shown in Figure S6). This indicates that the 3D cluster structures may become thermodynamically more favorable with the increase of cluster size, where smaller clusters show a tendency to maximize the interactions with the substrate. In general, the gas phase clusters are more spherical than the supported clusters, although the supported clusters also become more spherical as the particle size increases.

To further explore the effects of adsorbates, we conducted *in situ* XAS measurement at the Pt L_3 edge under the same conditions used for the *in situ* PDF experiments. The bond distances extracted from the XAS measurements were slightly smaller than those obtained from the PDF measurements. This phenomenon has been ascribed to anharmonic vibration of the surface atoms in the small nanoparticles at room temperature.[16] However, the contraction and relaxation of the Pt bond distances determined by fitting the EXAFS data were very similar to those of the PDF measurements (Table 2 and Figure S7). The Fourier transform data of the Pt-in-H_2 and Pt-in-CO were obtained at room temperature while Pt-in-He was at 250 °C, which is why the magnitude of Pt-in-He is lower. The fits,

dx.doi.org/10.1021/ja4126998 | J. Am. Chem. Soc. 2014, 136, 9320−9326

Table 2. L_3 EXAFS fits of Pt catalysts with and without adsorbed CO or H_2.[a]

	adsorbed gas	CN_{Pt-Pt}	R (Å)	DWF ($\times 10^3$)	E_0 (eV)
Pt foil	None (in He)	12	2.77	0.0	0.0
1c Pt	None (in He)	5.9	2.69	2.0	−1.6
	H_2	6.0	2.74	1.0	−2.3
	CO	6.0	2.76	1.0	−1.2
3c Pt	None (in He)	8.7	2.73	1.0	−0.1
	H_2	8.7	2.76	0.5	−0.8
	CO	8.5	2.76	1.0	−1.3
5c Pt	None (in He)	10.0	2.74	0.5	0.2
	H_2	10.2	2.76	0.5	−0.8
	CO	9.8	2.76	0.5	0.8

[a]EXAFS of Pt-in-He was taken at 250 C. CN is coordination numbers with error ±10%. R is bond distance with error ±0.02 Å. DWF is Debye−Waller factor. E_0 is energy shift. A two-shell model fit of the k^2-weighted EXAFS data was obtained between k = 2.9−11.7 $Å^{-1}$ and r = 1.3−2.8 Å.

however, indicate the same particle size in all three conditions, but with shorter bond distance for Pt-in-He. Additionally, PDF also shows there is no change in size with temperature or adsorbate (see Figure S4). The bond distance for the 1 nm Pt-in-He was 2.69 Å. With the adsorption of H_2 and CO, the bond distance relaxed to 2.74 and 2.76 Å, respectively. Similar trends were observed for the 2−3 nm Pt nanoparticles but the magnitude of the changes was smaller.

Changes in the electronic structure of small Pt nanoparticles caused by adsorbates may in turn change the Pt lattice parameters. XANES of the Pt L_3 edge represents a $2p \rightarrow 5d$ transition. As observed in previous studies, adsorption of H_2 and CO results in changes in the shape of the Pt L_3 XANES spectra.[15,45] Figure 7 shows the Pt L_3 edge for 1−3 nm Pt/Al_2O_3 with adsorbed H_2 and CO. The L_3 edge shifts to higher energy and the peaks broaden with adsorbed H_2 and CO. These changes are most significant for the smallest Pt particles. The ΔXANES (XANES of the Pt nanoparticles with the adsorbate minus that in He) has a negative peak at the edge (~11.564 keV) and a positive peak beyond the edge. The area of the positive peaks is suggested proportional to the H/Pt or CO/Pt ratio,[47,48] which we ascribe to differences in the Pt particle size and dispersion. Specifically, smaller Pt nanoparticles have higher H/Pt or CO/Pt ratio under the same conditions because they have a higher percentage of surface atoms. The higher H/Pt and CO/Pt ratio can cause a larger change in the electronic structure of Pt nanoparticles, which reflects as a larger ΔXANES spectrum.

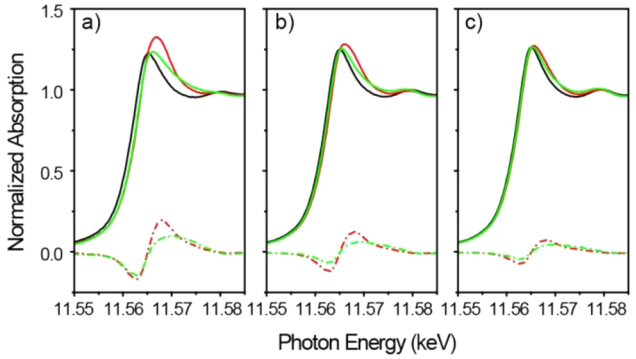

Figure 7. Normalized Pt L_3 XANES and ΔXANES of (a) 1c Pt/Al_2O_3, (b) 3c Pt/Al_2O_3, and (c) 5c Pt/Al_2O_3. Green in H_2, red in CO, black in He. Solid line, L_3 XANES; dash dot line, L_3 ΔXANES with respect to Pt-in-He.

Lattice contraction of very small particles has been attributed to changes in the hybridization of metal bonds at the surface that minimize the under-coordination of the surface atoms. [45] Consequently, the adsorption of H_2 and CO relaxes this lattice contraction in 1−3 nm Pt nanoparticles due to rehybridization of the metal orbitals. [15] Our PDF and XAS data suggest that the rehybridization caused by H_2 and CO are different, and this finding is consistent with previous DFT calculations.[49] In PDF measurements, the adsorption of CO on 1−3 nm Pt nanoparticles would lead to a longer Pt−Pt bond distance and less crystallinity compared to H_2 adsorption. In the XANES and ΔXANES measurements, the changes in L_3 edge are more significant when CO was adsorbed on Pt as compared to H_2. The difference in Pt-adsorbate bonding hybridization can be used to explain the PDF data. In the case of CO adsorption, it was suggested that the hybridization of d-orbitals is involved in back-donation to the CO π-bond. [15] In contrast, when hydrogen adsorbs on Pt, Pt-H antibonding states are formed with *s-d* coupling to stabilize the metal cluster *d* bonding state. The adsorption of H_2 produces a similar, but smaller effect than that with adsorbed CO in agreement with the previous reports.

CONLUSION

In conclusion, for 1−3 nm Pt nanoparticles supported over Al_2O_3, we have observed changes in the Pt lattice parameters upon adsorption of CO and H_2. *In situ* PDF measurements showed that the Pt−Pt bond distance contracts by ~1.4% at the surface of ~1 nm Pt-in-He nanoparticles. The 2−3 nm Pt nanoparticles showed similar but smaller changes due to the lower fraction of under-coordinated Pt surface atoms in larger Pt particles. The adsorption of H_2 and CO at room temperature relaxed Pt−Pt bond contraction to a value near that of bulk fcc Pt. Similar phenomena are confirmed by the *in situ* XAS study under the same conditions. The adsorption of H_2 improves the crystallinity of small Pt nanoparticles. However, with the adsorbed CO, *d*-PDF suggested a more disordered fcc structure for 1−3 nm Pt nanoparticles than for the Pt-in-He nanoparticles. This can be explained by the electron back-donation from Pt nanoparticles to the CO, leading to a higher degree of rehybridization of the metal orbitals in Pt-adsorbate systems. These findings will help us to understand adsorbate-induced structural and chemical changes in sub-3 nm Pt catalysts and be useful for improving catalytic activity.

ASSOCIATED CONTENT

Supporting Information

Additional PDFs fittings, EXAFS spectra and results of MD simulations. This material is available free of charge via the Internet at http://pubs.acs.org.

AUTHOR INFORMATION

Corresponding Author

jelam@anl.gov

Author Contributions

[¶]These authors contributed equally.

Notes

The authors declare no competing financial interest.

■ ACKNOWLEDGMENTS

This material is based upon work supported as part of the Institute for Atom-efficient Chemical Transformations (IACT), an Energy Frontier Research Center funded by the U.S. Department of Energy, Office of Science, Office of Basic Energy Sciences. Use of the Advanced Photon Source was supported by the U.S. Department of Energy, Office of Science, Office of Basic Energy Sciences, under Contract No. DE-AC02-06CH11357. MRCAT operations are supported by the Department of Energy and the MRCAT member institutions. This research was carried out in part at the Center for Functional Nanomaterials, Brookhaven National Laboratory, which is supported by the U.S. Department of Energy, Office of Basic Energy Sciences, under Contract No. DE-AC02-98CH10886. Y.L. gratefully acknowledges the start-up support by the University of Alabama in Huntsville. B.L. also thanks the start-up support by the Kansas State University. We acknowledge grants of computer time at the Argonne Laboratory Computing Resource Center (LCRC), and the National Energy Research Scientific Computing Center (NERSC).

■ REFERENCES

(1) Haruta, M. *Catal. Today* **1997**, *36* (1), 153−166.
(2) Argo, A. M.; Odzak, J. F.; Gates, B. C. *J. Am. Chem. Soc.* **2003**, *125* (23), 7107−7115.
(3) Guzman, J.; Carrettin, S.; Fierro-Gonzalez, J. C.; Hao, Y. L.; Gates, B. C.; Corma, A. *Angew. Chem., Int. Ed.* **2005**, *44* (30), 4778−4781.
(4) Lei, Y.; Mehmood, F.; Lee, S.; Greeley, J.; Lee, B.; Seifert, S.; Winans, R. E.; Elam, J. W.; Meyer, R. J.; Redfern, P. C.; Teschner, D.; Schlogl, R.; Pellin, M. J.; Curtiss, L. A.; Vajda, S. *Science* **2010**, *328* (5975), 224−228.
(5) Hagen, J. *Industrial Catalysis*; Wiley-VCH: Mannheim, 2006.
(6) Bartholomew, C. H.; Farrauto, R. J. *Fundamentals of Industrial Catalytic Processes*, 2nd ed.; Wiley-AIChE: New York, 2005.
(7) Tsung, C. K.; Kuhn, J. N.; Huang, W. Y.; Aliaga, C.; Hung, L. I.; Somorjai, G. A.; Yang, P. D. *J. Am. Chem. Soc.* **2009**, *131* (16), 5816−5822.
(8) Lennard-Jones, J. E.; Dent, B. M. *Proc. R. Soc. London, Ser. A* **1928**, *121*, 247−259.
(9) Bunn, C. W. *Proc. Phys. Soc.* **1935**, *47* (5), 835−842.
(10) Finch, G. I.; Fordham, S. *Proc. Phys. Soc.* **1936**, *48* (1), 85−94.
(11) Boswell, F. W. C. *Proc. Phys. Soc. A* **1951**, *64* (5), 465−476.
(12) Berry, C. R. *Phys. Rev.* **1952**, *88* (3), 596−599.
(13) Apai, G.; Hamilton, J. F.; Stohr, J.; Thompson, A. *Phys. Rev. Lett.* **1979**, *43* (2), 165−169.
(14) Miller, J. T.; Kropf, A. J.; Zha, Y.; Regalbuto, J. R.; Delannoy, L.; Louis, C.; Bus, E.; van Bokhoven, J. A. *J. Catal.* **2006**, *240* (2), 222−234.
(15) Lei, Y.; Jelic, J.; Nitsche, L. C.; Meyer, R.; Miller, J. T. *Top. Catal.* **2011**, *54*, 334−348.
(16) Hansen, L. B.; Stoltze, P.; Norskov, J. K.; Clausen, B. S.; Niemann, W. *Phys. Rev. Lett.* **1990**, *64* (26), 3155−3158.
(17) Bus, E.; Miller, J. T.; Kropf, A. J.; Prins, R.; van Bokhoven, J. A. *Phys. Chem. Chem. Phys.* **2006**, *8* (27), 3248−3258.
(18) Billinge, S. J. L.; Levin, I. *Science* **2007**, *316* (5824), 561−565.
(19) Proffen, T.; Billinge, S. J. L.; Egami, T.; Louca, D. *Z. Kristallogr.* **2003**, *218* (2), 132−143.
(20) Newton, M. A.; Chapman, K. W.; Thompsett, D.; Chupas, P. J. *J. Am. Chem. Soc.* **2012**, *134* (11), 5036−5039.
(21) Zhao, H. Y.; Nenoff, T. M.; Jennings, G.; Chupas, P. J.; Chapman, K. W. *J. Phys. Chem. Lett.* **2011**, *2* (21), 2742−2746.
(22) Elam, J. W.; Groner, M. D.; George, S. M. *Rev. Sci. Instrum.* **2002**, *73* (8), 2981−2987.
(23) Chupas, P. J.; Ciraolo, M. F.; Hanson, J. C.; Grey, C. P. *J. Am. Chem. Soc.* **2001**, *123* (8), 1694−1702.
(24) Hammersley, A. P.; Svensson, S. O.; Hanfland, M.; Fitch, A. N.; Hausermann, D. *High Pressure Res.* **1996**, *14* (4−6), 235−248.
(25) Farrow, C. L.; Juhas, P.; Liu, J. W.; Bryndin, D.; Bozin, E. S.; Bloch, J.; Proffen, T.; Billinge, S. J. L. *J. Phys.: Condens. Matter* **2007**, *19*, 33.
(26) Ilavsky, J.; Jemian, P. R.; Appl., J. *Crystallogr.* **2009**, *42*, 347−353.
(27) Smith, W.; Forester, T. R. *J. Mol. Graphics* **1996**, *14* (3), 136−141.
(28) Matsui, M. *Mineral. Mag.* **1994**, *58A*, 571−572.
(29) Rafiitabar, H.; Sutton, A. P. *Philos. Mag. Lett.* **1991**, *63* (4), 217−224.
(30) Sutton, A. P.; Chen, J. *Philos. Mag. Lett.* **1990**, *61* (3), 139−146.
(31) Levine, S. M.; Garofalini, S. H. *Surf. Sci.* **1986**, *167* (1), 198−206.
(32) Athanasopoulos, D. C.; Garofalini, S. H. *J. Chem. Phys.* **1992**, *97*, 3775−3780.
(33) King, J. S.; Wittstock, A.; Biener, J.; Kucheyev, S. O.; Wang, Y. M.; Baumann, T. F.; Giri, S. K.; Hamza, A. V.; Baeumer, M.; Bent, S. F. *Nano Lett.* **2008**, *8* (8), 2405−2409.
(34) Dasgupta, N. P.; Liu, C.; Andrews, S.; Prinz, F. B.; Yang, P. D. *J. Am. Chem. Soc.* **2013**, *135*, 12932−12935.
(35) Setthapun, W.; Williams, W. D.; Kim, S. M.; Feng, H.; Elam, J. W.; Rabuffetti, F. A.; Poeppelmeier, K. R.; Stair, P. C.; Stach, E. A.; Ribeiro, F. H.; Miller, J. T.; Marshall, C. L. *J. Phys. Chem. C* **2010**, *114* (21), 9758−9771.
(36) Lei, Y.; Liu, B.; Lu, J. L.; Lobo-Lapidus, R. J.; Wu, T. P.; Feng, H.; Xia, X. X.; Mane, A. U.; Libera, J. A.; Greeley, J. P.; Miller, J. T.; Elam, J. W. *Chem. Mater.* **2012**, *24* (18), 3525−3533.
(37) Aaltonen, T.; Ritala, M.; Tung, Y. L.; Chi, Y.; Arstila, K.; Meinander, K.; Leskela, M. *J. Mater. Res.* **2004**, *19* (11), 3353−3358.
(38) Chupas, P. J.; Chapman, K. W.; Jennings, G.; Lee, P. L.; Grey, C. P. *J. Am. Chem. Soc.* **2007**, *129* (45), 13822−13824.
(39) Chapman, K. W.; Chupas, P. J.; Kepert, C. J. *J. Am. Chem. Soc.* **2005**, *127* (32), 11232−11233.
(40) Chupas, P. J.; Chapman, K. W.; Chen, H. L.; Grey, C. P. *Catal. Today* **2009**, *145* (3−4), 213−219.
(41) Somorjai, G. A.; Park, J. Y. *Angew. Chem., Int. Ed.* **2008**, *47* (48), 9212−9228.
(42) Martinez-Inesta, M. A. M.; Lobo, R. F. *J. Phys. Chem. C* **2007**, *111* (24), 8573−8579.
(43) Egami, T.; Billinge, S. J. L. *Underneath the Bragg Peaks: Structural Analysis of Complex Materials*, 1st ed.; Pergamon: Amsterdam, 2003.
(44) Li, L.; Wang, L. L.; Johnson, D. D.; Zhang, Z. F.; Sanchez, S. I.; Kang, J. H.; Nuzzo, R. G.; Wang, Q.; Frenkel, A. I.; Li, J.; Ciston, J.; Stach, E. A.; Yang, J. C. *J. Am. Chem. Soc.* **2013**, *135*, 13062−13072.
(45) Bus, E.; van Bokhoven, J. A. *J. Phys. Chem. C* **2007**, *111* (27), 9761−9768.
(46) Ramallo-Lopez, J. M.; Santori, G. F.; Giovanetti, L.; Casella, M. L.; Ferretti, O. A.; Requejo, F. G. *J. Phys. Chem. B* **2003**, *107* (41), 11441−11451.
(47) Kubota, T.; Asakura, K.; Ichikuni, N.; Iwasawa, Y. *Chem. Phys. Lett.* **1996**, *256* (4−5), 445−448.
(48) Reifsnyder, S. N.; Otten, M. M.; Sayers, D. E.; Lamb, H. H. *J. Phys. Chem. B* **1997**, *101* (25), 4972−4977.
(49) Schweitzer, N.; Xin, H. L.; Nikolla, E.; Miller, J. T.; Linic, S. *Top. Catal.* **2010**, *53* (5−6), 348−356.